Available online at www.sciencedirect.com
ScienceDirect
Journal of the European Ceramic Society 31 (2011) 2915–2922
www.elsevier.com/locate/jeurceramsoc

Porous YSZ ceramics with unidirectionally aligned pore channel structure: Lowering thermal conductivity by silica aerogels impregnation

Liangfa Hu [a], Chang-An Wang *, Yong Huang

State Key Lab of New Ceramics and Fine Processing, Department of Materials Science and Engineering, Tsinghua University, Beijing 100084, PR China

Received 13 February 2011; received in revised form 21 June 2011; accepted 10 July 2011
Available online 3 August 2011

Abstract

The previous report of this work has demonstrated the fabrication and properties of porous yttria-stabilized zirconia (YSZ) ceramics with unidirectionally aligned pore channels. As a follow-up study, the present work aims at lowering the thermal conductivity of the porous YSZ ceramics by silica aerogels impregnation. The porous YSZ ceramics were immersed in an about-to-gel silica sol. Both the unidirectionally aligned pore channels and the inter-grain pores by grain stacking in the channel-pore wall of the porous YSZ ceramics were impregnated with the silica sol. After aging and supercritical drying, silica aerogels formed in the macroporous network of the porous YSZ ceramics with unidirectionally aligned pore channels. The influences of silica aerogel impregnation on the microstructure and properties of porous YSZ ceramics with unidirectional aligned pore channels were investigated. The porosity decreased after impregnation with silica aerogels. Both microstructure observation and pore size distribution indicated that both channel-pore size and inter-grain pore-size decreased significantly after impregnation with silica aerogels. Impregnating porous YSZ ceramics with silica aerogels remarkably lowered the room-temperature thermal conductivity and enhanced the compressive strength. The as-fabricated materials are thus suitable for applications in bulk thermal isolators.

Keywords: ZrO_2; Porosity; Thermal conductivity; Insulators

1. Introduction

Zirconia, which offers low thermal conductivity and good mechanical performance, is of great interest for insulated engine components, refractory and thermal insulation.[1] Furthermore, introducing pores into the zirconia materials decreases thermal conductivity, due to the air trapped in the pores creating a better thermal insulator. There is currently widespread interest in fabricating porous zirconia ceramics with low thermal conductivity for their applications in bulk thermal isolators. The fabrication methods include replication technique using polymeric sponge,[2] impregnation of open-cell polyurethane foams,[3] CNC-machining and slurry coating process,[4] using pore forming agents,[5] TBA-based gel-casting[6] and freeze casting.[7,8] All these methods have been successfully developed to fabricate porous zirconia ceramics and thus lower thermal conductivity. However, the strength of porous ceramics decreases significantly with increasing porosity, thus restricting their use. Although the primary function of the thermal insulation materials may not be structural, many of the applications require a certain degree of strength which is often absent in highly porous YSZ ceramics. Thus, lowering thermal conductivity while preserving strength becomes the threshold of developing porous zirconia ceramics as thermal insulation materials.

Aerogels could also be ideal materials for commercial thermal insulators due to their unique chemical and textural characteristics.[9–11] Many studies have long focused on aerogels due to their extraordinary properties, such as ultra-large specific surface area (500–1200 m^2/g), ultra-low density (0.003–0.35 g/cm^3), ultra-low thermal conductivity (0.012–0.1 W/mK), and ultra-high porosity, which originate from their mesoporous structure.[12–15] However, a distinctive characteristic of aerogels is that they are extremely brittle and weak, and aerogels generally have poor mechanical properties.[16] Improvement to the mechanical properties of aerogels was realized by reinforcing their mesoporous structure with

* Corresponding author. Tel.: +86 10 62785488; fax: +86 10 62785488.
E-mail addresses: lhu@tamu.edu (L. Hu), wangca@tsinghua.edu.cn (C.-A. Wang).
[a] Current address: Materials Science and Engineering Program, Texas A&M University, 3003 TAMU, College Station, TX 77843-3003, USA.

0955-2219/$ – see front matter © 2011 Elsevier Ltd. All rights reserved.
doi:10.1016/j.jeurceramsoc.2011.07.014

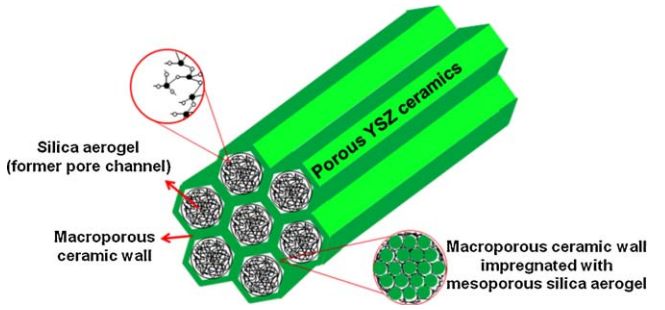

Fig. 1. Conceptual depiction of the porous YSZ ceramics impregnated with silica aerogels.

polymers.[17–21] Incorporating aerogels into other porous materials, however, was rarely reported.

Composite materials are one of the most important research fields in material science.[22] The advantage of composite materials is that they usually exhibit the best qualities of their components and some qualities that neither component possesses. It could be assumed that incorporating silica aerogels, a better thermal insulator than air, into the porous structure of porous zirconia ceramics would lower the thermal conductivity while further reinforcing the structure since the impregnation would reduce the pore size.

This work describes synthesis of a porous YSZ/silica aerogels composite material by impregnating porous YSZ ceramics with silica aerogels, in order to combine lower thermal conductivity and higher compressive strength in the as-prepared composite material. The synthesis of this composite material is depicted conceptually in Fig. 1, which shows porous YSZ ceramics with unidirectionally aligned pore channels impregnated with mesoporous silica aerogels. The objective of this work was twofold: the first was to further lower thermal conductivity by incorporating mesoporous silica aerogels into macroporous network of the porous YSZ ceramics with unidirectionally aligned pore channels; and the second was to enhance compressive strength by reinforcing the network matrix of porous YSZ ceramics with silica aerogels.

2. Experimental

2.1. Impregnating porous YSZ ceramics with silica aerogels

The porous YSZ ceramics with unidirectionally aligned pore channels were fabricated by freeze casting, using three different freezing agents which offer different freezing temperatures: chilled alcohol (CAH) with a temperature of −30 °C, solidified carbon dioxide (SCD) with a temperature of −78 °C and liquid nitrogen (LN2) with a temperature of −196 °C. The detailed fabrication procedure is described elsewhere.[7]

Fig. 2 shows the process of impregnating porous YSZ ceramics with silica aerogels. The silicon precursor, tetraethoxysilane (TEOS), was dissolved in methanol. Water containing NH_4OH as a catalyst was added into the solution while vigorously stirring. The mixture was poured into molds to immerse the porous YSZ ceramics with unidirectionally aligned pore channels which were previously set in the molds. The pressure in the molds was decreased to replace the air with the as-prepared solution in the pores of the porous YSZ ceramics. Wet gel formed in the macroporous network of the porous YSZ ceramics, both in the pore channels and in the inter-grain pores in the channel-pore wall, by hydrolysis and condensation within 12 h. The wet gel was then aged in a pure ethanol bath for 40 h, followed by a supercritical drying process which was performed in an autoclave with a diameter of 105 mm and a depth of 100 mm. The temperature and pressure in the autoclave were raised to 260 °C and 7.8 MPa, above the critical point of ethanol (T_c = 243 °C; p_c = 6.3 MPa),[23] respectively. The obtained silica aerogels were distributed in both the unidirectionally aligned pore channels and the inter-grain pores in the channel-pore wall of the porous YSZ ceramics.

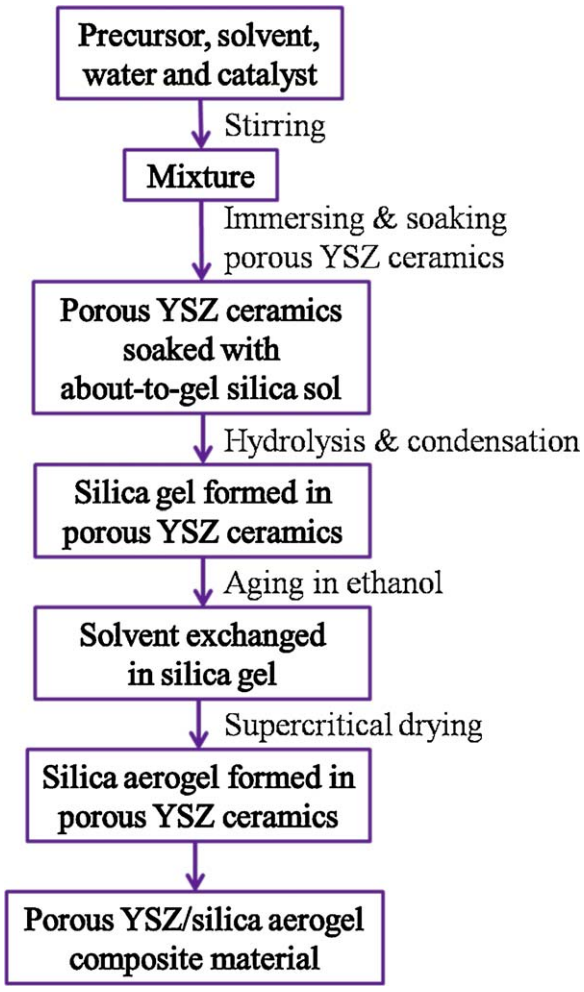

Fig. 2. Process flowchart of impregnating the porous YSZ ceramics with silica aerogels.

2.2. Characterization

The microstructure was observed using a scanning electron microscope (SEM, JSM 6700F, JEOL, Tokyo, Japan). Pore channel size was determined by measuring the size of pore channels from the microstructure of the section paralleled to

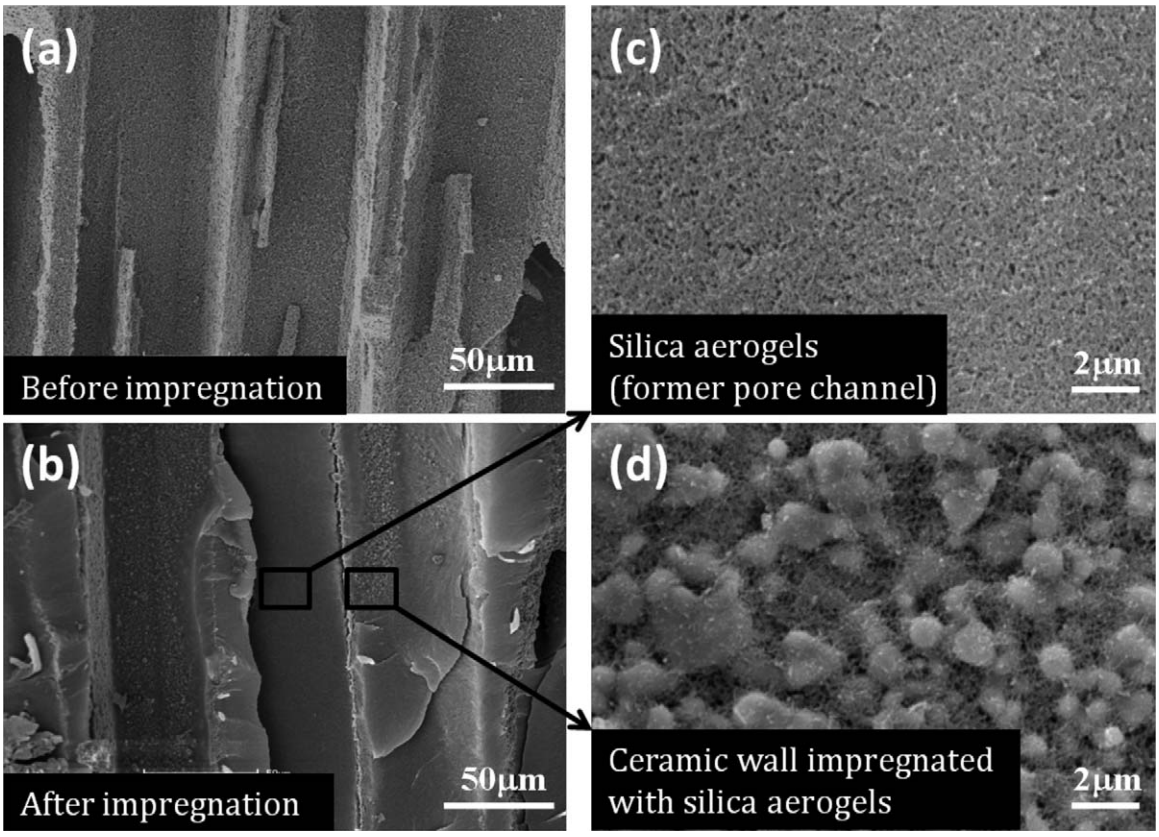

Fig. 3. SEM images of the porous YSZ ceramics with unidirectionally aligned pore channels before impregnation (a), after impregnation (b), silica aerogels (the former pore channel) (c) and ceramic wall impregnated with silica aerogels (d).

the cooled plate. The microstructure was taken at four randomly selected locations on each sample (two samples per condition). Pore size distribution of the porous YSZ ceramics with unidirectionally aligned pore channels was analyzed by a mercury intrusion porosimetry (AutoPore-IV9510, Micromeritics Instrument Corp., United States). The mesopores of the silica aerogels are hardly detectable with mercury intrusion method due to crushing of the silica aerogels during intrusion of mercury into the silica aerogels. For this reason, the average pore size distribution of silica aerogels was determined by N_2 adsorption at 77 K instead of mercury intrusion. Bulk density of the sintered samples before infiltration was measured from sample mass and dimension, and relative density, thus porosity were determined from the ratio of the measured bulk density to the theoretical one of the YSZ material, which was taken as 6.0 g/cm^3. Three samples were examined to determine the average porosity. The mass of the silica aerogel impregnated into the sample was calculated by subtracting the mass of the sample after impregnation by the corresponding mass before impregnation. The volume of the incorporated silica was obtained through dividing the mass by the density of the silica aerogel which was measured separately. The porosity of the sample after impregnation was then calculated through subtracting the original volume fraction of pores by the volume fraction that was occupied by the silica aerogel. Thermal conductivity at room temperature was measured on 5 mm × 5 mm × 3 mm machined specimens, using a Thermal Transport Option (TTO) of Physical Properties Measurement System (PPMS, Model 6000, Quantum Design, USA). The TTO system measured thermal conductivity λ by applying heat from the heater shoe in order to create a user-specified temperature differential (ΔT) between the two thermometer shoes, which were connected to the two sides of sample using epoxies (including silver-filled H20E and nonconductive tra-bond 816H01). TTO dynamically modeled the thermal response of the sample to the low-frequency, square-wave heat pulse, thus expediting data acquisition. TTO then calculated thermal conductivity directly from the applied heat power, resulting ΔT, and sample geometry. The compressive strength was measured by using a CSS-2220 testing machine with cylindrical specimens with a diameter of 20 mm and a height of 20 mm. Three specimens were used to determine the average compressive strength.

3. Results and discussion

3.1. Microstructure

Fig. 3 shows the microstructure of the porous YSZ ceramics with unidirectionally aligned pore channels before impregnation (a), after impregnation (b), silica aerogels (the former pore channel) (c) and ceramic wall impregnated with silica aerogels (d). The architectures were observed in the same section area parallel to the pore channels before and after impregnation (Fig. 3(a) and (b)), respectively. Compared to Fig. 3(a), impregnation with silica aerogels in the unidirectionally aligned pore

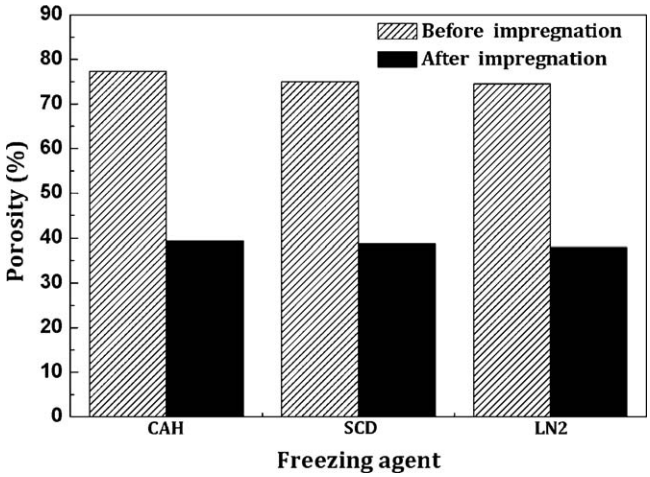

Fig. 4. Porosity of the porous YSZ ceramics with unidirectionally aligned pore channels before and after impregnation with silica aerogels. The porous YSZ ceramics were fabricated using three freezing agents: chilled alcohol (CAH), solidified carbon dioxide (SCD) and liquid nitrogen (LN2).

channels (~50 μm) of the porous YSZ ceramics was observed in Fig. 3(b). It was indicated in Fig. 3(b) that silica aerogels occupied most places of the pore channels, resulting in a significant decrease of pore channel size. Fig. 3(c) and (d) showed the microstructure of silica aerogels formed in the pore channels and the inter-grain pores in the channel-pore wall, respectively. It was noted that the mesopores of silica aerogels were much smaller than both pore channels and inter-grain pores in the channel-pore wall. Fig. 3 illustrated that three types of pores were found in the porous YSZ ceramics with unidirectionally aligned pore channels impregnated with silica aerogels: Type I, pore channels with channel size about 50 μm; Type II, inter-grain pores in the channel-pore wall with pore size around 1 μm; Type III, mesopores in the silica aerogels with nano-sized pores.

3.2. Porosity

Fig. 4 shows the porosity of porous YSZ ceramics with unidirectionally aligned pore channels before and after impregnation with silica aerogels. The porosity of the porous YSZ ceramics before impregnation was higher than that after impregnation. Fig. 3 demonstrated that silica aerogels occupied places in both pore channels and the inter-grain pores in the channel-pore wall. The loss of places in these pores resulted in a decrease of porosity in the porous YSZ ceramics. It should be noted that the decrease of porosity in the CAH sample was more than that in other two samples. It had been explained in the previous report[7] that CAH samples had the highest porosity among the three samples, which could also be seen in Figs. 4 and 5. Due to the highest porosity in the CAH samples, the most silica aerogels were impregnated into this sample, leading to the most decrease of porosity. As demonstrated in the previous report,[7] porosities of the porous YSZ ceramics both before and after impregnation with silica aerogels revealed a similar decreasing trend as the freezing temperature decreased.

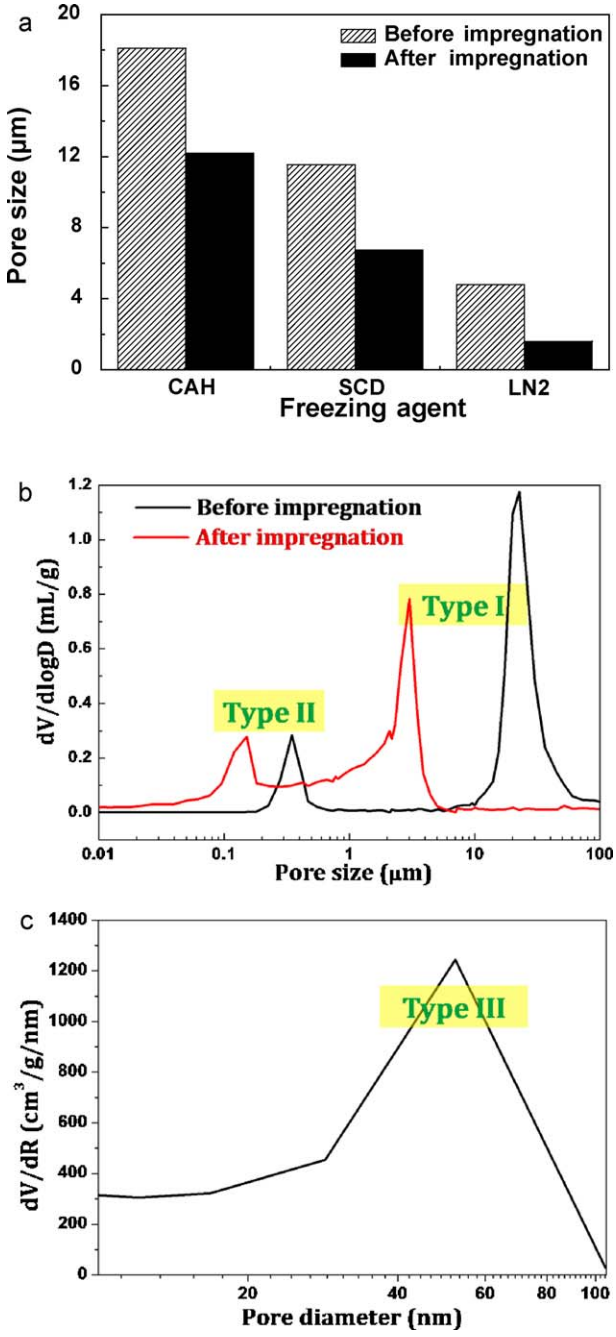

Fig. 5. (a) Mean pore size, (b) a typical pore size distribution determined by mercury intrusion method for the porous YSZ ceramics with unidirectionally aligned pore channels before and after impregnation with silica aerogels, (c) pore size distribution determined by N_2 adsorption at 77 K.

3.3. Pore size and distribution

Fig. 5(a) shows the mean pore size of the porous YSZ ceramics with unidirectionally aligned pore channels before and after impregnation with silica aerogels. The mean pore size of porous YSZ ceramics before was larger than that after impregnation. Fig. 3 demonstrated that silica aerogels occupied places in both pore channels and the inter-grain pores in the channel-pore wall. The loss of places in these pores resulted in a decrease of pore size, both pore channel size and the pore size of inter-grain pores

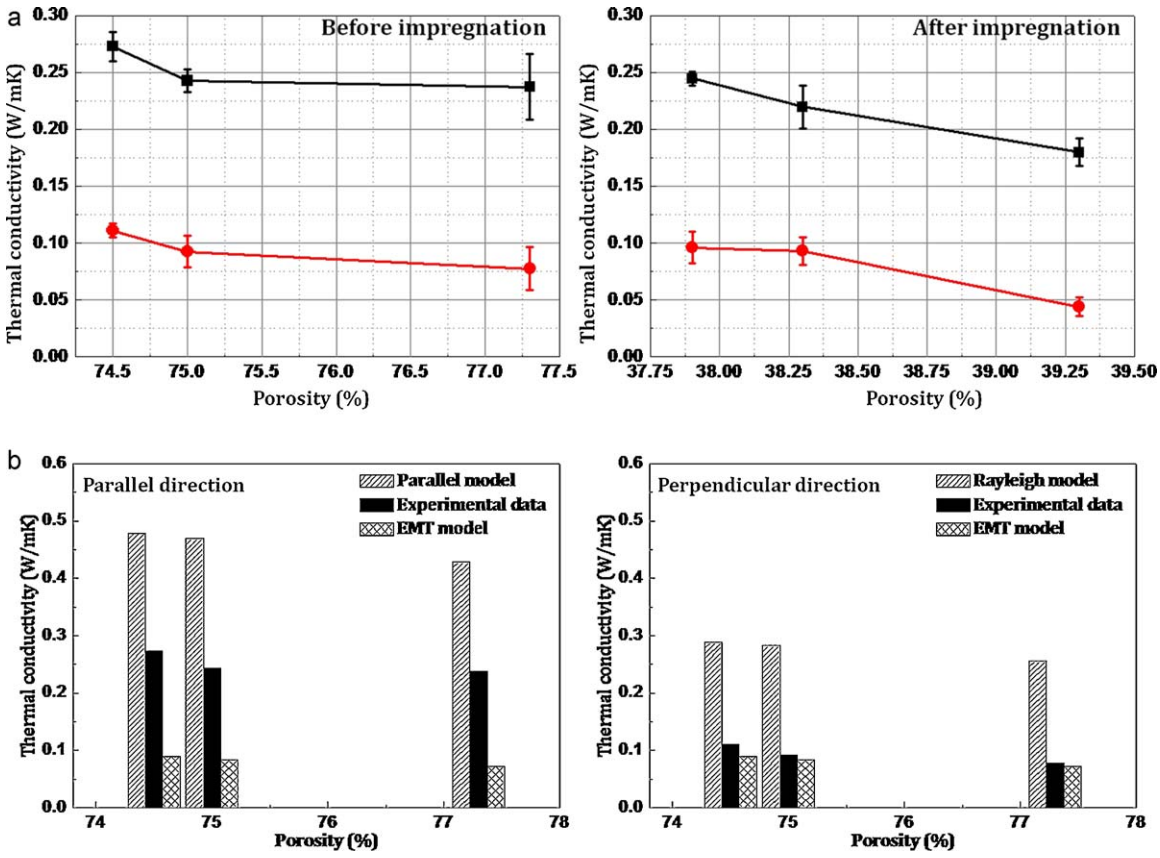

Fig. 6. (a) Room-temperature thermal conductivity of the porous YSZ ceramics with unidirectionally aligned pore channels before and after impregnation with silica aerogels. The thermal conductivity was tested along two directions: parallel direction ($\lambda_{\parallel}$) and perpendicular direction ($\lambda_{\perp}$). (b) Thermal conductivity of the porous YSZ ceramics with unidirectionally aligned pore channels: comparison of experimental data with calculated values derived from Rayleigh expression (perpendicular direction), parallel model (parallel direction) and EMT model (the fine interconnected pore structure).

in the channel-pore wall, of the porous YSZ ceramics. Both pore sizes of porous YSZ ceramics before and after impregnation revealed a similar decreasing trend as the freezing temperature decreased. The reasons had been demonstrated in the previous report.[7]

Fig. 5(b) shows a typical pore size distribution determined by mercury intrusion method for porous YSZ ceramics with unidirectionally aligned pore channels before and after impregnation with silica aerogels. Each case presented a bimodal pore size distribution with two peaks. One peak had a peak pore size of 0.35 μm and 0.15 μm before and after impregnation, respectively. These pores were created by both burn-out of binders and grain stacking in the ceramic wall, as shown in Fig. 3(d). The other peak was located at 23 μm and 3 μm before and after impregnation, respectively. These pores dominated most pore volume in all samples. They represented the unidirectionally aligned pore channels. Each peak revealed a narrow half-peak width, signifying a narrow pore size distribution. It could be seen in this figure that the pore channel size and the pore size of inter-grain pores in the channel-pore wall decreased from 23 μm and 0.35 μm to 3 μm and 0.15 μm, respectively. The result was consistent with that of Fig. 5(a). It should be noted that the pore size of the mesoporous silica aerogels was not observed in this figure. The authors believed that no intrusion of mercury into the silica aerogels was detected and only a crushing of the silica aerogels occurred when measurements were performed using the mercury intrusion method. Typically, aerogels can easily be compressed, in particular by the capillary stresses during adsorption or desorption in mercury porosimetry.[24]

Because the mesopores of the silica aerogels are hardly detectable with mercury intrusion method, the pore size distribution of silica aerogels was determined by N_2 adsorption at 77 K and then calculated using the KJS method.[25] The results were shown in Fig. 5(c), in which a single peak near 50 nm was observed. The single peak represented the mesopores in silica aerogels. It could be concluded that three types of pores were detected by pore size distribution determinations of the porous YSZ ceramics impregnated with silica aerogels. The results were consistent with the observations in Fig. 3.

3.4. Room-temperature thermal conductivity

Fig. 6 shows the room-temperature thermal conductivity of porous YSZ ceramics before and after impregnation with silica aerogels. All the samples had low thermal conductivities, 0.04–0.27 W/m K, which were much lower than that of dense YSZ ceramics (~1.8 W/m K). The reproducibility of the equipment was checked with a set of control experiments on the same silica aerogel specimen including 3 measurements of the thermal conductivity. The measured values were

0.018 W/m K, 0.020 W/m K and 0.023 W/m K, respectively. They had an average value 0.020 W/m K of and a deviation value of ±0.002 W/m K, respectively.

At a given porosity, the thermal conductivity of porous YSZ ceramics after impregnation was lower than that before impregnation. Particularly, after impregnating porous YSZ ceramics with silica aerogels, the thermal conductivities along the parallel direction ($\lambda_{\parallel}$) and perpendicular direction ($\lambda_{\perp}$) decreased from 0.24 to 0.28 W/m K and 0.08–0.11 W/m K to 0.18–0.24 W/m K and 0.04–0.09 W/m K, respectively. Both thermal conductivities of porous YSZ ceramics before and after impregnation with silica aerogels revealed a similar decreasing trend as the porosity increased. Meanwhile, the thermal conductivity in the perpendicular direction ($\lambda_{\perp}$) along the pore channel was lower than that in the parallel direction ($\lambda_{\parallel}$).

As a better thermal insulator than air (λ, 0.026 W/m K), silica aerogels replaced the air in both pore channels and the interparticle packing pores in the ceramic wall, which resulted in a decrease of thermal conductivity. The very low thermal conductivity of the silica aerogel could also be related to the Knudsen effect, which means that the gas molecules collide with the pore walls more frequently than with each other because the pore size (50 nm) in the silica aerogel is smaller than the mean free path of the diffusing gas molecules. The gas molecules within the matrix experienced the Knudsen effect, which virtually eliminated exchange of energy in the gas, effectively eliminating convection and lowering overall thermal conductivity. Solid phase conduction was low due to the low density and high surface area of the material.

The thermal conductivity along the perpendicular direction and the parallel direction could be modeled by the Rayleigh expression for two-phase component materials and parallel model, on the basis of the structural characteristics along these two measurement direction, respectively. The effective thermal conductivity λ_e of two-phase composite materials could be predicted by the Rayleigh expression[26]:

$$\lambda_e = \lambda_1 \left[\frac{\lambda_2 + \lambda_1 + v_2(\lambda_2 - \lambda_1)}{\lambda_2 + \lambda_1 - v_2(\lambda_2 - \lambda_1)} \right] \quad (1)$$

where λ_1 and λ_2 are the thermal conductivity of the two phases, 1 and 2, in the composite materials, and v_2 is the volume fraction of phase 2. Meanwhile, the Parallel model predicts the effective thermal conductivity of two-phase materials[27]:

$$\lambda_e = (1 - v_2)\lambda_1 + v_2\lambda_2 \quad (2)$$

where the symbols have same meaning with that in the Rayleigh expression.

On the basis of the two-phase parallel model (parallel direction) and the Rayleigh model (perpendicular direction), the calculated thermal conductivity values were given in Fig. 6(b) for comparison with the experimental data. The calculation used 1.8 $Wm^{-1} K^{-1}$ as λ_1 for the YSZ solid phase and 0.026 $Wm^{-1} K^{-1}$ as λ_2 as for the pores, resulting in calculated thermal conductivity values of porous YSZ sample with different porosities before impregnation. At a given porosity, the thermal conductivity predicted by the Rayleigh expression was lower than that predicted by the parallel model. It was consistent with the experimental data. Although the calculated and experimental results were not in exact agreement, the difference between the calculated values approached the difference in experimental results for the two measured directions. Meanwhile, the experimental data were lower than the values predicted from both Rayleigh expression and parallel model.

One reason why the experimental data were lower than the calculated values was that the fine interconnected pores among the channel walls took up considerable volume fraction of the overall pores. In the fine interconnected pore structure in which the two components are distributed connectively, either component may form continuous heat conduction pathways, depending on the relative amounts of the components. James[28] developed Landauer's theory[29] and pointed out that the effective conductivity of this type of structure could be modeled well by the effective medium theory (EMT) model:

$$(1 - v_2)\frac{k_1 - k_e}{k_1 + 2k_e} + v_2\frac{k_2 - k_e}{k_2 + 2k_e} = 0 \quad (3)$$

where the symbols have same meaning with that in the Rayleigh expression. Fig. 6(b) shows the calculated results for comparison with the experimental data. The values predicted from the EMT model were lower than the experimental data. This indicated that the fine interconnected pores among the channel walls which took up considerable volume fraction of the overall pores played an important role in lowering further the thermal conductivity, along the parallel and perpendicular direction, of the porous YSZ ceramics with unidirectionally aligned pore channels. Taking both the long pore channels (Rayleigh expression and parallel approaches) and the fine interconnected pores (EMT model) into account, the calculated values and the experimental data of thermal conductivity approached an agreement.

3.5. Compressive strength

Fig. 7 shows the compressive strength of porous YSZ ceramics with unidirectionally aligned pore channels before and after impregnation with silica aerogels. Due to the high porosity (>70%) which led to an exponential decrease of strength, the compressive strength of the porous YSZ ceramics in the present work, 0.3–8.6 MPa, was much lower than the corresponding value (2068 MPa)[c] of dense zirconia ceramics. The compressive strength of porous YSZ ceramics after impregnation with silica aerogels was much higher than that before impregnation. Particularly, after impregnating porous YSZ ceramics with silica aerogels, the compressive strength along the parallel direction ($\sigma_{\parallel}$) and perpendicular direction ($\sigma_{\perp}$) increased from 0.9 to 3.9 MPa and 0.3–1.7 MPa to 7.4–8.6 MPa and 1.8–2.7 MPa, respectively. Decreased porosity and pore size, as well as stiffened network by impregnation with silica aerogels contributed to the increased compressive strength of porous YSZ ceramics impregnated with silica aerogels. Meanwhile, the compressive strength tested along the parallel direction ($\sigma_{\parallel}$) was higher than that along the perpendicular direction ($\sigma_{\perp}$).

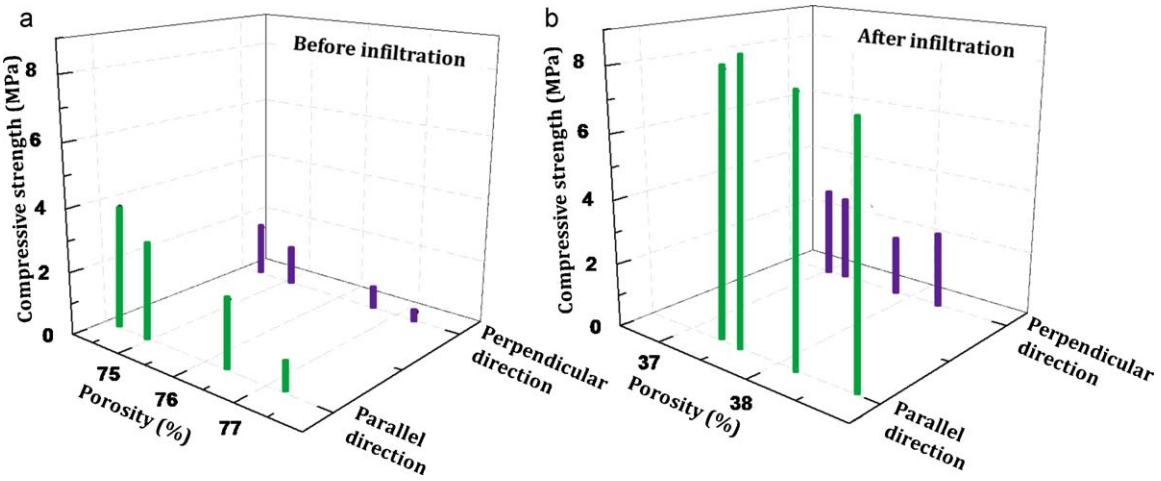

Fig. 7. Compressive strength of the porous YSZ ceramics with unidirectionally aligned pore channels before and after impregnation with silica aerogels. The compressive strength was tested along two directions: parallel direction ($\sigma_{\parallel}$) and perpendicular direction ($\sigma_{\perp}$).

4. Conclusions

The impregnation of porous YSZ ceramics with silica aerogels resulted in a porous YSZ/silica aerogels composite material that had tri-modal pores: pore channels, inter-grain stacking pores and mesopores in the silica aerogels. Porosity decreased after impregnation with silica aerogels. Both pore channel size and the pore size of inter-grain pores in the channel-pore wall of porous YSZ ceramics with unidirectionally aligned pore channels decreased significantly after impregnation. The room-temperature thermal conductivity of porous YSZ ceramics was further lowered while the compressive strength was obviously improved. The as-prepared material was thus suitable to be applied in thermal insulations at ambient conditions, such as freezers, refrigerators, heat storage and transport system.

Acknowledgements

This work was supported by the National Natural Science Foundation of China (Grant No: 90816019), the Natural High Technology Research and Development Program of China ("863" Program, Grant No: 2007AA03Z435) and State Key Development Program of Basic Research of China ("973" program, Grant No: 2006CB605207-2).

References

1. Claussen N, Ruhle M, Heuer A. *Science and technology of zirconia II*. Columbus: The American Ceramic Society, Inc.; 1983.
2. Kim HW, Lee SY, Bae CJ, Noh YJ, Kim HE, Kim HM, Ko JS. Porous ZrO_2 bone scaffold coated with hydroxyapatite with fluorapatite intermediate layer. *Biomaterials* 2003;**24**:3277–84.
3. Gomez SY, Escobar JA, Alvarez OA, Rambo CR, de Oliveira APN, Hotza D. ZrO_2 foams for porous radiant burners. *Journal of Materials Science* 2009;**44**:3466–71.
4. Jun IK, Koh YH, Song JH, Lee SH, Kim HE. Fabrication and characterization of dual-channeled zirconia ceramic scaffold. *Journal of the American Ceramic Society* 2006;**89**:2021–6.
5. Nait-Ali B, Haberko K, Vesteghem H, Absi J, Smith DS. Thermal conductivity of highly porous zirconia. *Journal of the European Ceramic Society* 2006;**26**:3567–74.
6. Hu L, Wang CA, Huang Y. Porous yttria-stabilized zirconia ceramics with ultra-low thermal conductivity. *Journal of Materials Science* 2010;**42**:3242–6.
7. Hu L, Wang CA, Huang Y, Sun C, Lu S, Hu Z. Control of pore channel size during freeze casting of porous YSZ ceramics with unidirectionally aligned channels using different freezing temperatures. *Journal of the European Ceramic Society* 2010;**30**:3389–96.
8. Hong C, Zhang X, Han J, Du J, Zhang W. Camphene-based freeze-cast ZrO_2 foam with high compressive strength. *Materials Chemistry and Physics* 2010;**119**:359–62.
9. Pajonk GM. Some applications of silica aerogels. *Colloid and Polymer Science* 2003;**281**:637–51.
10. Rigacci A, Marechal JC, Repoux M, Moreno M, Achard P. Preparation of polyurethane-based aerogels and xerogels for thermal superinsulation. *Journal of Non-Crystalline Solids* 2004;**350**:372–8.
11. Wei TY, Chang TF, Lu SY, Chang YC. Preparation of monolithic silica aerogels of low thermal conductivity by ambient pressure drying. *Journal of the American Ceramic Society* 2007;**90**:2003–7.
12. Husing N, Schubert U. Aerogels-airy materials: chemistry, structure and properties. *Angewandte Chemie – International Edition* 1998;**37**:22–45.
13. Gesser HD, Goswami PC. Aerogels and related porous materials. *Chemical Reviews* 1989;**89**:765–88.
14. Pierre AC, Pajonk GM. Chemistry of aerogels and their applications. *Chemical Reviews* 2002;**102**:4243–66.
15. Fricke J, Emmerling A, Aerogels. *Journal of the American Ceramic Society* 1992;**75**:2027–35.
16. Ma HS, Roberts AP, Prevost JH, Jullien R, Scherer GW. Mechanical structure–property relationship of aerogels. *Journal of Non-Crystalline Solids* 2000;**277**:127–41.
17. Oskam G, Searson PC. Sol–gel synthesis and characterization of carbon/ceramic composite electrodes. *Journal of Physical Chemistry* 1998;**102**:2464–8.
18. Fujiki K, Ogasawara T, Tsubokawa N. Preparation of a silica gel–carbon black composite by the sol–gel process in the presence of polymer-grafted carbon black. *Journal of Materials Science* 1998;**33**:1871–9.
19. Liu R, Shi Y, Wan Y, Meng Y, Zhang F, Gu D, Chen Z, Tu B, Zhao D. Triconstituent co-assembly to ordered mesostructured polymer-silica and carbon–silica nanocomposites and large-pore mesoporous carbons with high surface areas. *Journal of the American Ceramic Society* 2006;**128**:11652–62.
20. Glover TG, Dunne KI, Davis RJ, LeVan MD. Carbon-silica composite adsorbent: characterization and adsorption of light gases. *Microporous and Mesoporous Materials* 2008;**111**:1–11.
21. Leventis N, Sotiriou-Leventis C, Zhang G, Rawashdeh AMM. Nanoengineering strong silica aerogels. *Nano Letters* 2002;**2**:957–60.

22. Jones RM. *Mechanics of composite materials*. 2nd ed. Philadelphia: Taylor & Francis; 1999.
23. Matson DW, Smith RD. Supercritical fluid technologies for ceramic-processing applications. *Journal of the American Ceramic Society* 1989;**72**:871–81.
24. Scherer GW, Smith DM, Qiu X, Anderson JM. Proceedings of the fourth international symposium on aerogels (ISA-4). *Journal of Non-Crystalline Solids* 1995;**186**:316–20.
25. Kruk M, Jaroniec M, Sayari A. Application of large pore MCM-41 molecular sieves to improve pore size analysis using nitrogen adsorption measurements. *Langmuir* 1997;**13**:6267–73.
26. Rayleigh L. On the influence of obstacles arranged in rectangular order upon the properties of a medium. *Philosophical Magazine* 1892;**34**:481–507.
27. Bart GCJ. Thermal conduction in non-homogeneous and phase change media. Thesis, Delft University of Technology, Netherlands; 1994.
28. James KC, Simon JL, David JT, Andrew CC. Thermal conductivity bounds for isotropic, porous materials. *International Journal of Heat and Mass Transfer* 2005;**48**:2150–8.
29. Landauer R. The electrical resistance of binary metallic mixtures. *Journal of Applied Physics* 1952;**23**:779–84.